ACS OMEGA

http://pubs.acs.org/journal/acsodf

Article

Pyrolysis Kinetic Analysis of Sequential Extract Residues from Hefeng Subbituminous Coal Based on the Coats-Redfern Method

Xian-Jin Huang, Wen-Long Mo,* Ya-Ya Ma, Xiao-Qiang He, Yelixiati Syls, Xian-Yong Wei,* Xing Fan, Xiao-Qin Yang, and Shu-Pei Zhang

Cite This: *ACS Omega* 2022, 7, 21397−21406

Read Online

ACCESS | Metrics & More | Article Recommendations

ABSTRACT: Sequential extract residues (R_i, i = 1, 2, 3, 4, and 5) were obtained from Hefeng acid-washing coal (HF_{AC}) by petroleum ether, carbon disulfide, methanol, acetone, and isometric carbon disulfide/acetone mixture, sequentially. Pyrolysis behavior of the residues was determined using thermogravimetry analysis. The Coats−Redfern method with different reaction orders was used to analyze the pyrolysis kinetic of each sample, and the kinetic parameters, including correlation coefficient (R^2), activation energy (E), and pre-exponential factor (A), were calculated. Results showed that the weight loss of extract residues was higher than HF_{AC}, and pyrolysis behavior varies greatly for residues, which is related to the unstable structure after extraction. From conversion−temperature ($\alpha-T$) curves, the pyrolysis process was divided into three stages: low-temperature stage (150−350 °C), medium-temperature stage (350−550 °C), and high-temperature stage (550−950 °C). The medium-temperature stage made great contribution to the process of pyrolysis, which was dominated by depolymerization and decomposition reaction. The relationship between kinetic parameters and reaction order showed that the swelling effect is an important reason for the discrepancy of E for each sample in the process of pyrolysis.

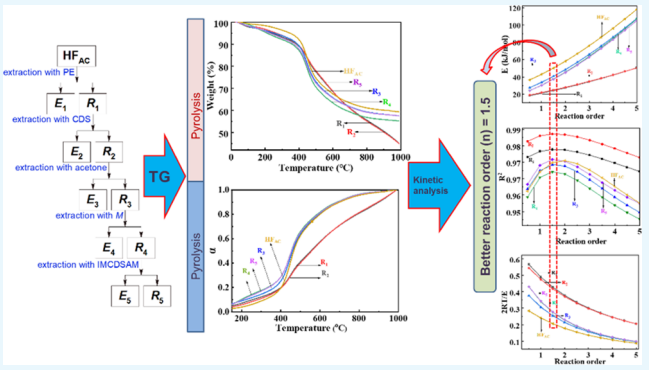

1. INTRODUCTION

In recent years, increasing consumption of coal, the main energy source in China, has caused serious environmental pollution problems. However, coal still plays a leading role in Chinese primary energy consumption for a long time in the future. Therefore, clean and efficient utilization of coal has become the top priority.[1,2] Solvent extraction under mild conditions can separate organic matter from coal by the principle of similar phase dissolution, without damaging the environment. The structure and composition characteristics of coal can be reflected by analyzing the molecular structure of the soluble molecules.[3,4] There are five kinds of intermolecular forces in coal, including entanglement interaction between alkyl and alkyl groups, $\pi-\pi$ interaction between aromatic rings, weak hydrogen bonds, strong hydrogen bonds, and hydrogen bond/$\pi-\pi$ complex interaction.[5,6] Different solvents can selectively break the intermolecular interaction in low-rank coal.[7−9] Therefore, sequential extraction with different solvents can effectively improve the extraction efficiency of organic matter in coal.

Macrokinetics is widely used in the study of coal pyrolysis characteristics and reaction mechanism, which shows high theoretical and practical significance for improving clean and efficient utilization of coal.[10,11] Thermogravimetric analysis (TGA) is a kind of thermal analysis technology, which measures the change of material quality with temperature and time in a controlled environment. This method has a lot of advantages, such as simple pretreatment, no reagent, and application.[12,13] By the establishment of the kinetic model, the pyrolysis process of coal can be quantitatively analyzed, which is convenient to understand the pyrolysis characteristics and mechanism of coal. Many theoretical models, including zero-order empirical model, single reaction model, multistage reaction model, and distributed activation energy model (DAEM), have been put forward by researchers.[14] In addition, many methods for calculating kinetic parameters are proposed according to the abovementioned model, including Coats−Redfern method, Kissinger method, Ozawa method, and Doyle method.[15] However, a universal model and method has not been developed due to the complexity and difference of the coal structure. Among them, a single reaction model, which

Received: January 15, 2022
Accepted: March 3, 2022
Published: June 16, 2022

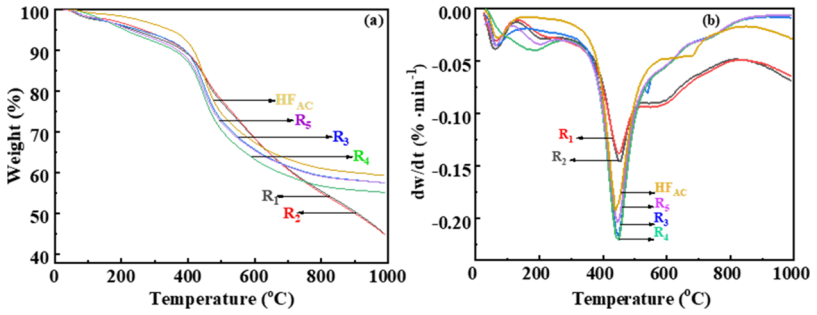

Figure 1. TG-DTG diagram of the samples: (a) TG profiles and (b) DTG profiles.

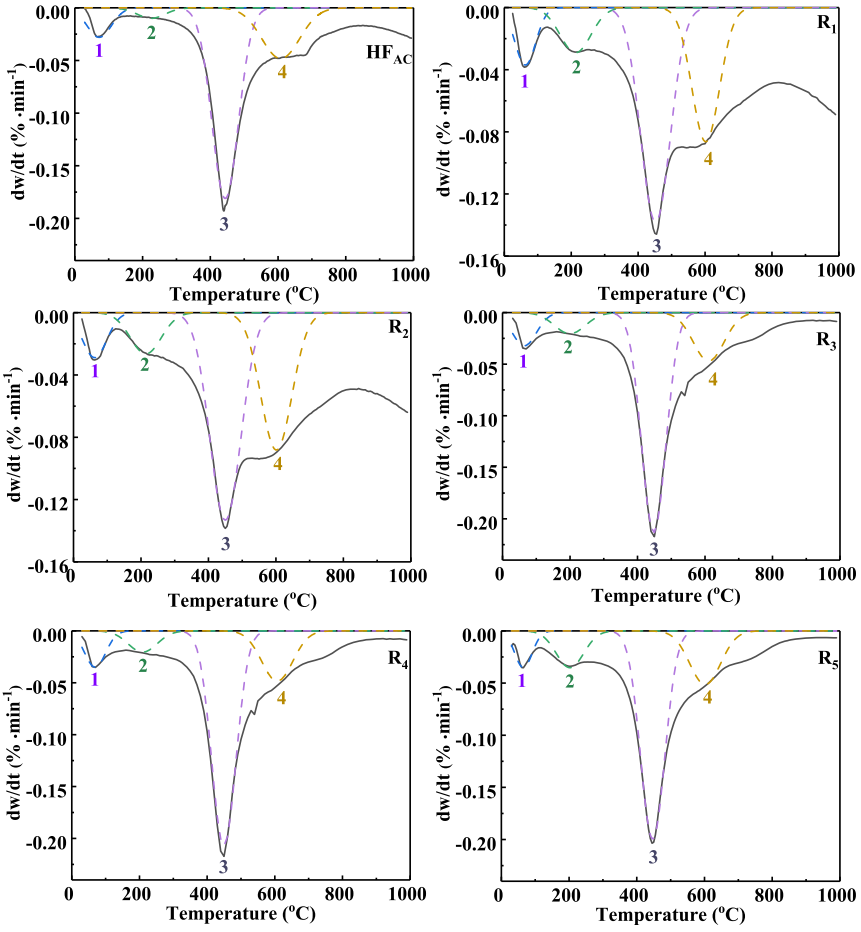

Figure 2. DTG and the peak fitting diagram of the samples.

considered the process of coal pyrolysis as an approximately first-order or *n*-order reaction and can well predict the kinetic parameters, has been widely concerned.[16]

Liu et al.[17] found that small coal particle size could enhance the surface heating rate, resulting in higher heat flux and lower activation energy. According to TGA, Geng et al.[18] reported that the pyrolysis process of Shenmu bituminous coal involved many types of covalent and other chemical bonds, resulting in the fact that the cleavage of each bond needs different activation energies. Du et al.[19] reported the pyrolysis kinetics of Shenfu coal, and the pyrolysis process could be divided into three stages. The low-temperature stage was contributed by small molecules of gas and water, and a large amount of gas and tar were evaporated in the middle-temperature region. Wu et al.[20] found that the well effect can be obtained in the violent pyrolysis stage for Xinjiang bituminous coal as the reaction order $n = 2$, and the reaction order $n = 1$ is suitable for the polycondensation and secondary cracking stage.

In this paper, pyrolysis kinetics of Xinjiang Hefeng acid-washing coal (HF_{AC}) and its sequential extract residues from petroleum ether (PE), carbon disulfide (CDS), methanol (*M*), acetone, and isometric acetone/carbon disulfide (IMCDSAM) were discussed under the reaction order of $n = 1-5$ with the single reaction model by the Coats−Redfern method.

2. RESULTS AND DISCUSSION

2.1. TG Analysis. Figure 1 shows TG and DTG profiles of Hefeng acid-washing coal and its extract residues. It can be seen from Figure 1a that there are significant differences in TG profiles for the samples. HF_{AC} shows a smaller weight loss of 41.03%, indicating that more coke is produced after the

https://doi.org/10.1021/acsomega.2c00307
ACS Omega 2022, 7, 21397−21406

Table 1. Proximate and Ultimate Analyses (wt %, daf) of the Samples[a]

	proximate analysis				ultimate analysis						
sample	M_{ad}	A_d	V_{daf}	FC_{daf}*	C	H	N	$S_{t,d}$	O*	H/C	O/C
HF	5.88	21.18	42.81	57.19	74.91	5.65	1.50	0.37	17.57	0.91	0.13
HF_{AC}	1.52	1.84	44.37	55.63	73.05	5.33	1.50	0.38	19.74	0.88	0.15

[a]daf: dry and ash-free base; *: by difference; and $S_{t,d}$: total sulfur (dry base).

Table 2. Fitting Results of DTG Curves[a]

	peak 1		peak 2		peak 3		peak 4	
sample	P_T (°C)	P_P (%)	P_T (°C)	P_P (%)	P_T (°C)	P_A (%)	P_P (°C)	P_A (%)
HF_{AC}	80	9.26	208	4.97	444	64.83	611	20.94
R_1	70	9.48	213	10.06	452	50.20	602	30.26
R_2	72	8.36	214	10.78	450	49.25	601	31.61
R_3	75	9.73	206	7.92	448	62.24	611	20.11
R_4	75	9.36	209	7.59	449	63.91	607	19.14
R_5	70	7.68	203	12.15	447	60.27	602	19.89

[a]P_T: peak temperature and P_A: peak area proportion.

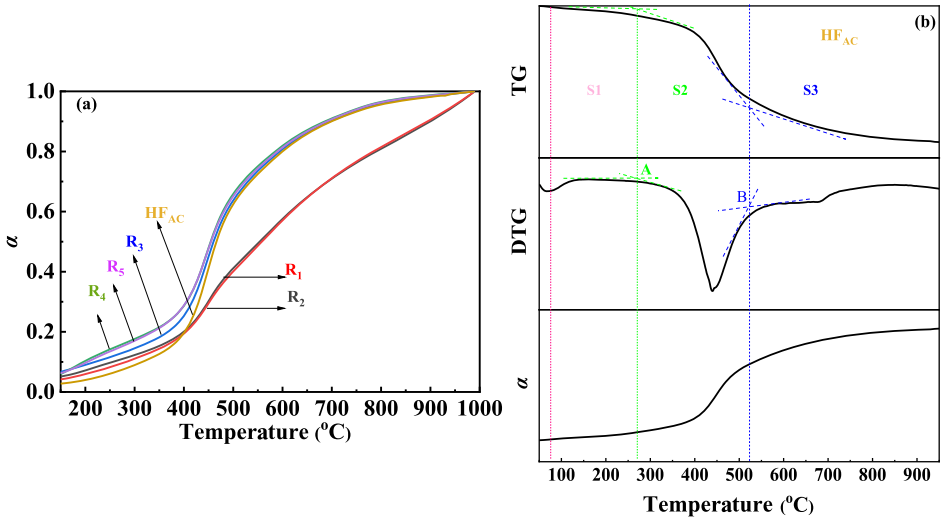

Figure 3. Diagram of conversion to temperature. (a): $\alpha-T$ and (b): TG/DTG/$\alpha-T$.

pyrolysis process. TG profiles of R_1 and R_2 are basically the same, with weight losses of 54.97 and 55.02%, respectively. TG profiles of R_3, R_4, and R_5 also present little difference, with weight losses of 42.33, 44.92, and 42.53%, respectively. When temperature is lower than 350 °C, the weight loss of each sample is about 10%. This stage might be mainly ascribed to the desorption of water and the small molecule gases, accounting for 18−25% of the weight loss. In addition, the weight loss of the residues was larger than that of HF_{AC}, which might be derived from the fact that after solvent extraction, the molecular structure of coal is unstable and some solvents remain in the residues. Temperature from 350 to 550 °C is the main thermal decomposition stage, which may belong to depolymerization and decomposition of larger molecular structural compounds in coal. Polycondensation reaction of aromatic rings might generate some gases (methane and its homologues, olefins, water, etc.) at a higher temperature range.

It can be seen from DTG curves in Figure 1b that the weight loss rate of R_1 and R_2 is smaller than that of HF_{AC}. This phenomenon may be due to the fact that volatile substances are dissolved into the extractant after primary and secondary solvent extraction, leading to a more stable molecular skeleton structure to the residues. Moreover, some solvents may enter into the pores of the coal molecular structure to form surface tension, which makes the pyrolysis process more difficult. While the weight loss rate of R_3, R_4, and R_5, from DTG profiles, is larger than that of HF_{AC}, which might be due to the influence of swelling on the structure after many times solvent extraction, the volume expansion might also take place to accelerate the process of pyrolysis.[21] When temperature is higher than 550 °C, aromatic rings condense, and aromatic nuclei increase, and semicoke forms coke rock. The weight loss of R_1 and R_2 is the largest in this stage, which could be related to the polycondensation reaction, releasing a large amount of small molecular gases. The reason for the small weight loss of R_3, R_4, and R_5 might be inferred that the macromolecular channels formed by swelling rapidly collapse under high-temperature conditions.

Figure 2 shows the DTG and its peak fitting curves of the samples. The DTG peaks can be considered as the energy required for the cleavage of different covalent bonds. Four peaks were fitted at different temperature regions, and the fitting details are listed in Table 2. Peak 1 occurs at about 70 °C, which could be related to the evaporation of water and

https://doi.org/10.1021/acsomega.2c00307
ACS Omega 2022, 7, 21397−21406

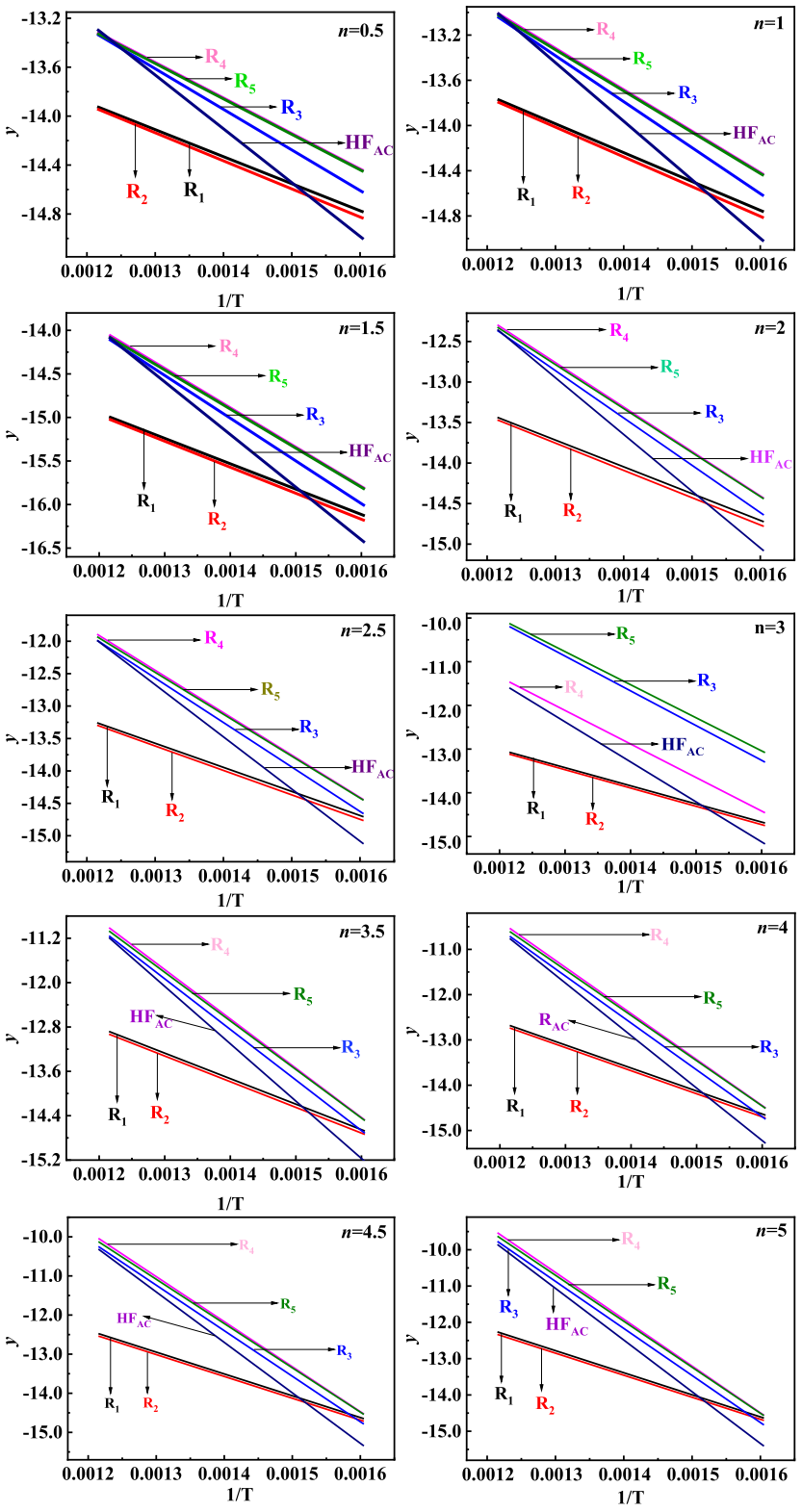

Figure 4. Fitting curves of each sample with reaction order n = 0.5−5.

small molecular gases. Peak 2, appearing at about 210 °C, might be related to the breakage of weak covalent bonds, such as >C_{al}−O<, >C_{al}−N<, and >C_{al}−S−.[22] The weak covalent bonds presented a smaller peak area proportion, demonstrating that the number of organic compounds containing this type of bonds is smaller. The assignment of peak 3 around 450 °C, which is caused by the breakage of stronger bonds, such as >C_{al}−C_{al}< and >C_{al}−S−. The peak area proportion of peak 3 is larger, indicating that a severe pyrolysis reaction occurred in this temperature region. Peak 4 appears around 605 °C, which may be ascribed to the reaction of carbonate decomposition or aromatic ring condensation and release of some small molecules.[23] The peak area proportion of peak 4 shows a considerable difference of Hefeng acid-washing coal and its

https://doi.org/10.1021/acsomega.2c00307
ACS Omega 2022, 7, 21397−21406

Table 3. Kinetic Parameters of Each Sample with Different Reaction Orders

n	sample	y	R^2	E (kJ/mol)	A (min^{-1})	2RT/E
0.5	R_1	$-2208.3x - 11.23$	0.9751	18.36	0.290	0.5642
	R_2	$-2293.3x - 11.15$	0.9819	19.07	0.328	0.5433
	R_3	$-3317.2x - 9.30$	0.9616	27.58	3.032	0.3756
	R_4	$-2901.1x - 9.78$	0.9582	24.12	1.625	0.4295
	R_5	$-2897.9x - 9.80$	0.9636	24.09	1.603	0.4300
	HF_{AC}	$-4396.1x - 7.95$	0.9607	36.55	15.517	0.2834
1	R_1	$-2550.2x - 10.67$	0.9776	21.20	0.592	0.4886
	R_2	$-2629.0x - 10.60$	0.9842	21.86	0.657	0.4739
	R_3	$-4065.4x - 8.10$	0.9693	33.80	12.370	0.3065
	R_4	$-3660.8x - 8.56$	0.9665	30.44	7.024	0.3404
	R_5	$-3645.2x - 8.59$	0.9717	30.31	6.769	0.3418
	HF_{AC}	$-5176.4x - 6.72$	0.9689	43.04	62.766	0.2407
1.5	R_1	$-2915.3x - 11.45$	0.9784	24.24	0.310	0.4274
	R_2	$-2986.8x - 11.39$	0.9850	24.83	0.337	0.4172
	R_3	$-4906.2x - 8.14$	0.9719	40.79	14.313	0.2540
	R_4	$-4521.9x - 8.56$	0.9689	37.60	8.680	0.2755
	R_5	$-4490.04x - 8.62$	0.9742	37.33	8.122	0.2775
	HF_{AC}	$-6045.5x - 6.73$	0.9728	50.26	72.047	0.2061
2	R_1	$-3303.5x - 9.42$	0.9782	27.47	2.673	0.3772
	R_2	$-3366.5x - 9.38$	0.9848	27.99	2.848	0.3701
	R_3	$-5838.1x - 5.27$	0.9714	48.54	300.202	0.2134
	R_4	$-5482.6x - 5.63$	0.9680	45.58	196.161	0.2273
	R_5	$-5430.6x - 5.72$	0.9734	45.15	177.238	0.2294
	HF_{AC}	$-7002.13x - 3.84$	0.9737	58.22	1498.491	0.1779
2.5	R_1	$-3714.6x - 8.74$	0.9773	30.88	5.917	0.3354
	R_2	$-3767.9x - 8.72$	0.9838	31.33	6.168	0.3307
	R_3	$-6856.1x - 3.66$	0.9689	57.00	1772.461	0.1817
	R_4	$-6536.9x - 3.95$	0.9653	54.35	1258.422	0.1906
	R_5	$-6461.6x - 4.08$	0.9710	53.72	1092.653	0.1928
	HF_{AC}	$-8041.9x - 2.22$	0.9723	66.86	8768.087	0.1549
3	R_1	$-4147.8x - 8.03$	0.9760	34.49	13.461	0.3004
	R_2	$-4190.41x - 8.02$	0.9824	34.84	13.715	0.2973
	R_3	$-7953.5x - 0.53$	0.9655	66.13	4.668×10^4	0.1567
	R_4	$-7676.7x - 2.14$	0.9618	63.82	9.066×10^3	0.1623
	R_5	$-7575.5x - 0.92$	0.9678	62.98	3.015×10^4	0.1645
	HF_{AC}	$-9158.8x - 0.47$	0.9697	76.15	5.719×10^4	0.1360
3.5	R_1	$-4602.6x - 7.29$	0.9744	38.27	31.466	0.2707
	R_2	$-4633.4x - 7.30$	0.9807	38.52	31.297	0.2689
	R_3	$-9121.74x - 0.07$	0.9618	75.84	8.471×10^4	0.1366
	R_4	$-8891.9x - 0.21$	0.9581	73.93	7.237×10^4	0.1401
	R_5	$-8762.9x - 0.42$	0.9643	72.85	5.744×10^4	0.1422
	HF_{AC}	$-10344.9 - 1.38$	0.9663	86.01	4.113×10^5	0.1204
4	R_1	$-5077.9x - 6.51$	0.9726	42.22	75.506	0.2454
	R_2	$-5096.0x - 6.55$	0.9788	42.37	73.238	0.2445
	R_3	$-10352.0x - 1.87$	0.9582	86.07	6.694×10^5	0.1204
	R_4	$-10172.4x - 1.83$	0.9547	84.57	6.311×10^5	0.1225
	R_5	$-10014.2x - 1.56$	0.9611	83.26	4.774×10^5	0.1244
	HF_{AC}	$-11592.5 - 3.33$	0.9627	96.38	3.222×10^5	0.1075
4.5	R_1	$-5572.9x - 5.70$	0.9709	46.33	185.805	0.2236
	R_2	$-5577.4x - 5.76$	0.9769	46.37	175.587	0.2234
	R_3	$-11635.7x - 3.89$	0.9547	96.74	5.689×10^6	0.1071
	R_4	$-11508.1x - 3.94$	0.9515	95.68	5.931×10^6	0.1083
	R_5	$-11320.1x - 3.63$	0.9581	94.11	4.271×10^6	0.1101
	HF_{AC}	$-12893.5x - 5.35$	0.9591	107.20	2.719×10^6	0.0966
5	R_1	$-6086.2x - 4.87$	0.9691	50.60	468.268	0.2047
	R_2	$-6076.5x - 4.95$	0.9750	50.52	430.764	0.2051
	R_3	$-12964.9x - 5.98$	0.9517	107.79	5.144×10^7	0.0961
	R_4	$-12890.1x - 6.13$	0.9488	107.17	5.933×10^7	0.0967
	R_5	$-12671.9x - 5.77$	0.9555	105.35	4.066×10^7	0.0983
	HF_{AC}	$-14240.3x - 7.45$	0.9556	118.39	2.445×10^8	0.0875

https://doi.org/10.1021/acsomega.2c00307
ACS Omega 2022, 7, 21397−21406

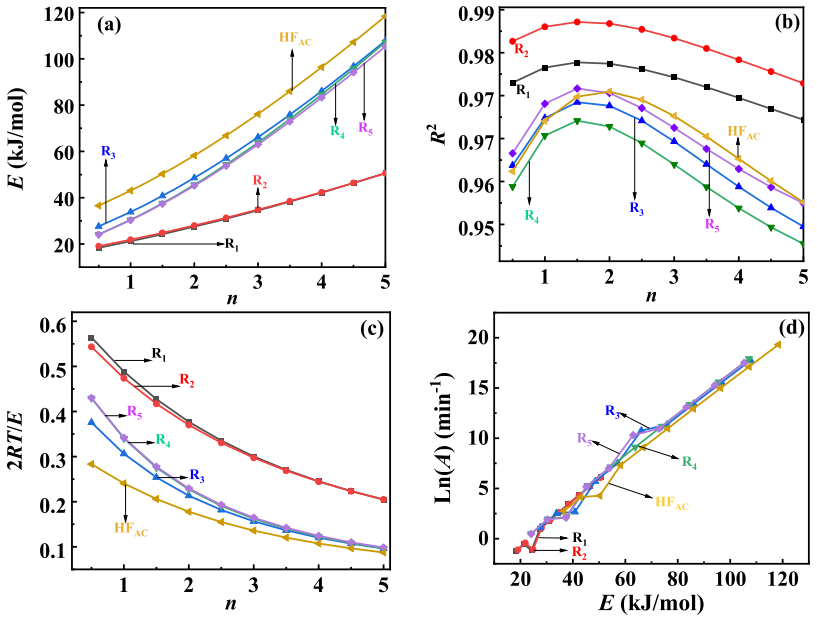

Figure 5. Relationship between kinetic parameters and reaction order. (a): $E-n$; (b): R^2-n; (c): $2RT/E-n$; and (d): $\ln(A)-E$.

extract residues. R_1 and R_2 present a larger peak area proportion at this temperature region.

2.2. Conversion−Temperature Diagram. Figure 3a shows the relationship between conversion and temperature of Hefeng acid-washing coal and its extract residues. It can be seen that there is little difference for the conversion−temperature profiles of the samples. Combining TG-DTG profiles with the $\alpha-T$ diagram, the pyrolysis process can be divided into three stages,[24,25] as shown in Figure 3b. The samples contain a small amount of moisture, and so, the weight loss below 150 °C is taken as the initial pyrolysis process. The intersection point A of the tangent line of TG and DTG profiles is taken as the dividing temperature point of the first stage (S1, 150−350 °C) and B as the second stage (S2, 350−550 °C), and the third stage (S3) ranged from 550−950 °C. It can be seen from Figure 3a that the change trend of conversion profiles is basically consistent in the stage of S1. The conversions of the residues are higher than that of HF_{AC}, which may be due to the fact that the residues contained more small molecules (Figure 1a). In the stage of S2, the conversions increase rapidly, which may be due to the fact that this temperature region is the main stage of pyrolysis reaction, and a large number of substances are depolymerized and decomposed. Moreover, the conversion profiles are divergent in this temperature range, that is, the increasing trend of R_3, R_4, R_5, and HF_{AC} is more obvious. In the stage of S3, the conversion of R_3, R_4, R_5, and HF_{AC} increases slowly, indicating that the pyrolysis process gradually becomes gentle, which may be because the main reaction of polycondensation is difficult to take place in this stage.

2.3. Coats−Redfern Kinetic Analysis. The Coats−Redfern method is suitable for analysis of the reactions with the single stage. The stage of S2 is the main process of pyrolysis reaction. Thus, kinetic fitting of each sample in the temperature range of 350−550 °C was carried out by the Coats−Redfern method to discuss the pyrolysis kinetic characteristics of the samples. The fitting diagram of reaction order n = 0.5−5 was obtained, as shown in Figure 4. It can be seen that each reaction order has little effect on R_1 and R_2, which may be due to the fact that the samples have a stable and similar structure. Our previous work[35] showed that the extraction process has a better effect to obtain organic matter from coal, while it does not change the main structure of coal. The fitting curves of R_3, R_4, R_5, and HF_{AC} have a large deviation when n = 3, indicating that different reaction orders can obviously affect the fitting effect.

2.4. Calculation of Kinetic Parameters. According to the fitting curves, the kinetic parameters, including regression equation (y), correlation coefficient (R^2), activation energy (E), and pre-exponential factor (A), were calculated under different reaction orders by the Coats−Redfern method, as shown in Table 3.

It can be seen that the values of R^2 are above 0.9500, indicating that the fitting correlation of each sample is better. Activation energy can reflect the difficulty of pyrolysis reaction. It is not difficult to see that the variation for activation energy is very large after extraction. Residues presented lower activation energy than HF_{AC}, indicating that coal after extraction is more conducive to pyrolysis. The pre-exponential factor is a constant determined by the nature of the reaction. Many studies[26−28] have found that the pre-exponential factor has a great difference under different reaction conditions. The value of the pre-exponential factor increases with the increase of the heating rate and reaction order, and it is also found that there is a "compensation effect" between the activation energy and pre-exponential factor. The Coats−Redfern integral formula assumes that the term E/RT is far greater than 1. Therefore, the smaller $2RT/E$ value could meet the preconditions of the formula, which means the better reliability of kinetic parameters.

2.5. Relationship between Kinetic Parameters and Reaction Order. Pyrolysis is a macroscopic process, and kinetic parameters can reflect the comprehensive performance of pyrolysis reaction. The higher reaction order means that the pyrolysis process is more complex. The relationship between kinetic parameters and reaction order in the temperature range of 350−550 °C is shown in Figure 5.

https://doi.org/10.1021/acsomega.2c00307
ACS Omega 2022, 7, 21397−21406

Figure 5a shows the relationship between the activation energy and reaction order. It can be seen from Figure 5a that activation energy increases with the increases of the reaction order for each sample, indicating that the higher the reaction order is, the more difficult the pyrolysis reaction is, while activation energy presents a significant difference for HF_{AC} and its residues, which could be related to the composition and structure difference of each sample after sequential extraction. Ma et al.[29] found that the coal sample showed the swelling effect in solvent, which is a process of gradual expansion, microexplosion, pore collapse, and formation of fragments. After the process of ultrasonic-assisted sequential extraction, with the pore structure of coal collapse, with weak bridge bond breaking and cross-linked network structure relaxing, the extract residues could be swelled under different solvents. Therefore, the swelling effect might be an important reason for the discrepancy of activation energy for each sample in the process of pyrolysis.

Figure 5b shows the relationship between the correlation coefficient R^2 and reaction order. The values of R^2 were all above 0.95, indicating that the correlation effect was acceptable. The correlation coefficient R^2 increases first and then decreases with the increase of the reaction order. The value of R^2 for HF_{AC} reaches the maximum of 0.9720 when the reaction order n = 2, while the values of the all residues reach the maximum when the reaction order n = 1.5.

Figure 5c shows the relationship between $2RT/E$ and reaction order. $2RT/E$ is the precondition for the calculation of kinetic parameters for the Coats−Redfern method. The lower the value, the higher the reliability of the model is. It can be seen that the value of $2RT/E$ decreases with the increase of the reaction order, indicating that the high reaction order can better meet the condition of the Coats−Redfern method.

Literatures[30−32] found that the pre-exponential factor increases when activation energy increases, and the factor decreases when the activation energy decreases, which is called "dynamic compensation effect". Meng et al.[33] also discovered that there was "dynamic compensation effect" between the activation energy and pre-exponential factor in the process of coal gasification, and the gas diffusion has a significant impact on the compensation effect.

The "dynamic compensation effect" can be expressed by a mathematical formula as follows[34]

$$\ln(A) = qE + p \quad (1)$$

where q and p are the compensation parameters.

In order to further explore the compensation effect of the activation energy and pre-exponential factor, the diagram of $\ln(A)-E$ is plotted, as shown in Figure 5d. It can be found that the relationship between the activation energy and pre-exponential factor is almost a line. There is a one-to-one correspondence between the activation energy and the reaction order, which could be used to predict the activation energy and the pre-exponential factor under the higher reaction order.

3. CONCLUSIONS

In this paper, thermogravimetric analyses of acid-washing coal and its extract residues were carried out. Results showed that the weight losses of all stages for extract residues were higher than that of HF_{AC}. The Coats−Redfern method was used to analyze the pyrolysis kinetics under the reaction order of n = 0.5−5 at the temperature stage of S2. The fitting effect is better because the correlation coefficient R^2 is above 0.95. Relationship between the kinetic parameters and reaction order showed that the swelling effect might be an important reason for the discrepancy of activation energy for each sample in the process of pyrolysis and the high reaction order can better meet the condition of Coats−Redfern method. $\ln(A)-E$ relationship can be used to predict the activation energy and the pre-exponential factor under the higher reaction order.

4. EXPERIMENTAL SECTION

4.1. Coal Sample. The used subbituminous coal sample was selected from Hefeng, Xinjiang, China. Table 1 shows the proximate and ultimate analyses of Hefeng coal (HF) and its acid-washing sample by mixtures of hydrochloric acid and hydrofluoric acid.

It can be seen from Table 1 that HF shows the characteristics of high ash, high volatile matter, high ratio of hydrogen to carbon and low sulfur. After acid-washing treatment, the ash content in HF_{AC} is greatly reduced, from 21.18 to 1.84%, with the removal rate high of 91.31%, indicating that acid-washing can effectively remove ash in coal. Thus, we can ignore the effect of ash and study the pyrolysis characteristics of organic matter in coal.

4.2. Sequential Extraction Process. The detailed process of the aid-washing step is reported in previous publications of our group.[35,36] HF_{AC} was successively extracted with petroleum ether (PE), carbon disulfide (CDS), methanol (M), acetone, and isometric acetone/carbon disulfide (IMCDSAM) by ultrasonic-assisted five-stage extraction. Residues obtained from each stage were recorded as R_i (i = 1, 2, 3, 4, 5), and the sequential extraction process is shown in Figure 6. The

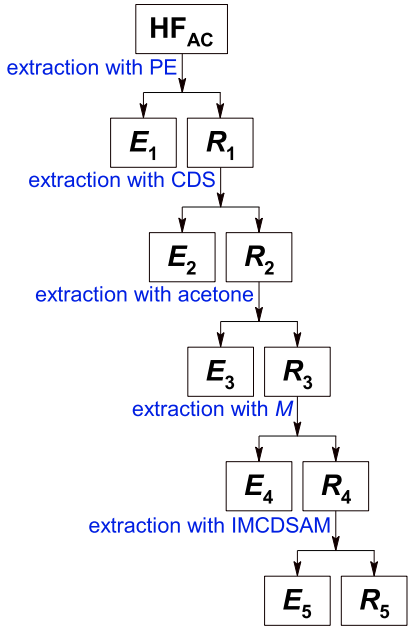

Figure 6. Sequential extraction process of HF_{AC}.

yield, structural characteristics, and composition distribution of the extract have been described in the literature,[37] and the residual yields of extract residues are shown in Figure 7.

4.3. Thermogravimetric Analysis. With N2 as the carrier gas, the pyrolysis behavior of HFAC and R_i (i = 1, 2, 3, 4, 5) was carried out on a thermogravimetric analyzer SDT-Q600 from TA company. The temperature was raised from ambient to 1000 °C, with a heating rate of 10 °C/min.

https://doi.org/10.1021/acsomega.2c00307
ACS Omega 2022, 7, 21397−21406

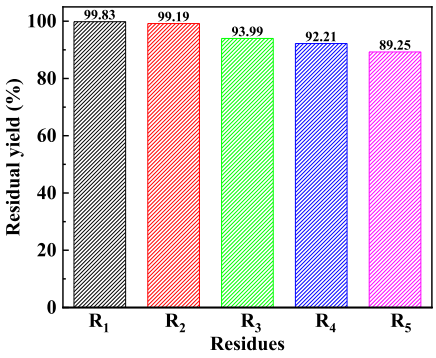

Figure 7. Residual yields of the extract residues.

4.4. Pyrolysis Kinetics Analysis. The pyrolysis kinetics of each sample was studied by conversion and other parameters. In this experiment, the Coats−Redfern method was used to calculate the kinetics parameters for the process of pyrolysis with a single heating rate.

According to the Coats−Redfern method, it generally has the following expression

When $n = 1$

$$\ln\left[-\frac{\ln(1-\alpha)}{T^2}\right] = \ln\left[\frac{AR}{\varphi E}\left(1-\frac{2RT}{E}\right)\right] - \frac{E}{RT} \quad (2)$$

when $n \neq 1$

$$\ln\left[\frac{1-(1-\alpha)^{1-n}}{T^2(1-n)}\right] = \ln\left[\frac{AR}{\varphi E}\left(1-\frac{2RT}{E}\right)\right] - \frac{E}{RT} \quad (3)$$

where α is the conversion; n is the reaction order; E is the activation energy, kJ/mol; T is the kelvin temperature, K; φ is the heating rate, K/min; R is the constant, 8.314 J/(mol·K); and A is the pre-exponential factor, min^{-1}.

According to the thermogravimetric analysis, the conversion is expressed as follows

$$\alpha = \frac{m_0 - m_g}{m_0 - m_f} \quad (4)$$

where m_g is the mass of the sample at a certain time (or temperature), m_g; m_0 is the initial mass of the sample, m_g; and m_f is the ending mass of the sample reaction, m_g.

Eqs 1 and 2 are analyzed. Generally, for most reaction temperature regions and most E, the term of $E/RT \geq 1$, $2RT/E \rightarrow 0$. Hence, $(1 - 2RT/E) \approx 1$, then eqs 1 and 2 can be simplified as follows

$$\ln\left[-\frac{\ln(1-\alpha)}{T^2}\right] = \ln\left(\frac{AR}{\varphi E}\right) - \frac{E}{RT} \quad (5)$$

$$\ln\left[\frac{1-(1-\alpha)^{1-n}}{T^2(1-n)}\right] = \ln\left(\frac{AR}{\varphi E}\right) - \frac{E}{RT} \quad (6)$$

When $n = 1$, let $y = \ln\left[-\frac{\ln(1-\alpha)}{T^2}\right]$; when $n \neq 1$, let $y = \ln\left[\frac{1-(1-\alpha)^{1-n}}{T^2(1-n)}\right]$; let $x = \frac{1}{T}$.

When n takes different reaction orders and plot y against x, and the regression equation is carried out, with the slope of $-E/R$ and the intercept of $\ln(AR/\varphi E)$. Activation energy and pre-exponential factor of the reaction can be calculated according to the regression equation.

AUTHOR INFORMATION

Corresponding Authors

Wen-Long Mo − *State Key Laboratory of Chemistry and Utilization of Carbon-Based Energy Resources and Key Laboratory of Coal Clean Conversion & Chemical Engineering Process (Xinjiang Uyghur Autonomous Region), College of Chemical Engineering, Xinjiang University, Urumqi, Xinjiang 830046, China;* orcid.org/0000-0003-3837-0915; Email: mowenlong@xju.edu.cn

Xian-Yong Wei − *State Key Laboratory of Chemistry and Utilization of Carbon-Based Energy Resources and Key Laboratory of Coal Clean Conversion & Chemical Engineering Process (Xinjiang Uyghur Autonomous Region), College of Chemical Engineering, Xinjiang University, Urumqi, Xinjiang 830046, China; Key Laboratory of Coal Processing and Efficient Utilization, Ministry of Education, China University of Mining & Technology, Xuzhou 221116 Jiangsu, China;* orcid.org/0000-0001-7106-4624; Email: wei_xianyong@163.com

Authors

Xian-Jin Huang − *State Key Laboratory of Chemistry and Utilization of Carbon-Based Energy Resources and Key Laboratory of Coal Clean Conversion & Chemical Engineering Process (Xinjiang Uyghur Autonomous Region), College of Chemical Engineering, Xinjiang University, Urumqi, Xinjiang 830046, China;* orcid.org/0000-0003-0947-6411

Ya-Ya Ma − *State Key Laboratory of Chemistry and Utilization of Carbon-Based Energy Resources and Key Laboratory of Coal Clean Conversion & Chemical Engineering Process (Xinjiang Uyghur Autonomous Region), College of Chemical Engineering, Xinjiang University, Urumqi, Xinjiang 830046, China*

Xiao-Qiang He − *State Key Laboratory of Chemistry and Utilization of Carbon-Based Energy Resources and Key Laboratory of Coal Clean Conversion & Chemical Engineering Process (Xinjiang Uyghur Autonomous Region), College of Chemical Engineering, Xinjiang University, Urumqi, Xinjiang 830046, China;* orcid.org/0000-0001-9714-2571

Yelixiati Syls − *State Key Laboratory of Chemistry and Utilization of Carbon-Based Energy Resources and Key Laboratory of Coal Clean Conversion & Chemical Engineering Process (Xinjiang Uyghur Autonomous Region), College of Chemical Engineering, Xinjiang University, Urumqi, Xinjiang 830046, China*

Xing Fan − *State Key Laboratory of Chemistry and Utilization of Carbon-Based Energy Resources and Key Laboratory of Coal Clean Conversion & Chemical Engineering Process (Xinjiang Uyghur Autonomous Region), College of Chemical Engineering, Xinjiang University, Urumqi, Xinjiang 830046, China; College of Chemical and Biological Engineering, Shandong University of Science and Technology, Qingdao, Shandong 266590, China*

Xiao-Qin Yang − *Xinjiang Yihua Chemical Industry Co., Ltd., Changji 831700, China*

Shu-Pei Zhang − *Xinjiang Yihua Chemical Industry Co., Ltd., Changji 831700, China*

Complete contact information is available at: https://pubs.acs.org/10.1021/acsomega.2c00307

https://doi.org/10.1021/acsomega.2c00307
ACS Omega 2022, 7, 21397−21406

Notes

The authors declare no competing financial interest.

■ ACKNOWLEDGMENTS

This work was supported by the Tianchi project for introducing high-level talents to Xinjiang Uyghur Autonomous Region (China), Key Laboratory of Coal Processing and Efficient Utilization from Ministry of Education and Open Project of Key Laboratory of Xinjiang Uygur Autonomous Region (Grant 2018D04008).

■ REFERENCES

(1) Tahmasebi, A.; Yu, J.; Han, Y.; Yin, F.; Bhattacharya, S.; Stokie, D. Study of chemical structure changes of Chinese lignite upon drying in superheated steam, microwave, and hot air. *J. Energy Fuels* **2012**, *26*, 3651−3660.

(2) Kong, J.; Wei, X.-Y.; Li, Z.-K.; Yan, H.-L.; Zhao, M.-X.; Zong, Z.-M. Identification of organonitrogen and organooxygen compounds in the extraction residue from Buliangou subbituminous coal by FTICRMS. *J. Fuel* **2016**, *171*, 151−158.

(3) Lei, Z.; Zhang, Y.; Wu, L.; Shui, H.; Wang, Z.; Ren, S. The dissolution of lignite in ionic liquids. *J. RSC Adv.* **2013**, *3*, 2385−2389.

(4) Liu, F.-J.; Wei, X.-Y.; Xie, R.-L.; Wang, Y.-G.; Li, W.-T.; Li, Z.-K.; Li, P.; Zong, Z.-M. Characterization of oxygencontaining species in methanolysis products of the extraction residue from Xianfeng lignite with negative-ion electrospray ionization Fourier transform ion cyclotron resonance mass spectrometry. *J. Energy Fuel.* **2014**, *28*, 5596−5605.

(5) Liu, F.-J.; Zong, Z.-M.; Li, W.-T.; Zhu, X.-N.; Wei, X.-Y.; Tang, M.-C.; Huang, Z.-X. A three-step dissociation method for converting Xiaolongtan lignite into soluble organic compounds: Insights into chemicals, geochemical clues, and structural characteristics. *J. Fuel* **2019**, *242*, 883−892.

(6) He, X.-Q.; Mo, W.-L.; Wang, Q.; Ma, Y.-Y.; Ma, F.-Y.; Fan, X.; Wei, X.-Y. Effect of swelling treatment by organic solvent on the structure and pyrolysis performance of the direct coal liquefaction residue. *J. Energy Fuel.* **2020**, *34*, 8685−8696.

(7) Hu, R.-n.; Wang, Z.-c.; Li, L.; Wang, X.-l.; Pan, C.-x.; Kang, S.-g.; Ren, S.-b.; Lei, Z.-p.; Shui, H.-f. Effect of solvent extraction pretreatments on the variation of macromolecular structure of low rank coals. *J. Fuel Chem. Technol.* **2018**, *46*, 778−786.

(8) Lv, J.-H.; Wei, X.-Y.; Wang, Y.-H.; Wang, T.-M.; Liu, J.; Zhang, D.-D.; Zong, Z.-M.; Ma, F.-Y.; Liu, J.-M. Mass spectrometric analyses of biomarkers and oxygen-containing species in petroleum ether-extractable portions from two Chinese coals. *J. Fuel* **2016**, *173*, 260−267.

(9) Shui, H.; Zhou, Y.; Li, H.; Wang, Z.; Lei, Z.; Ren, S.; Pan, C.; Wang, W. Thermal dissolution of Shenfu coal in different solvents. *J. Fuel* **2013**, *108*, 385−390.

(10) Heydari, M.; Rahman, M.; Gupta, R. Kinetic study and thermal decomposition behavior of lignite coal. *J. Int. J. Chem. Eng.* **2015**, *2015*, 1−9.

(11) Song, H.; Liu, G.; Zhang, J.; Wu, J. Pyrolysis characteristics and kinetics of low rank coals by TG-FTIR method. *J. Fuel Pro. Tech.* **2017**, *156*, 454−460.

(12) Guo, Y. H.; Cheng, F. Adaptability analysis of kinetic model of blended coal pyrolysis. *J. Combust. Sci. Technol.* **2019**, *25*, 509−518.

(13) Wu, D.; Liu, G.; Sun, R. Investigation on structural and thermodynamic characteristics of perhydrous bituminous coal by Fourier transform infrared spectroscopy and thermogravimetry/mass spectrometry. *J. Energy Fuel.* **2014**, *28*, 3024−3035.

(14) Ojha, D. K.; Viju, D.; Vinu, R. Fast pyrolysis kinetics of lignocellulosic biomass of varying compositions. *Energy Convers. Manage.: X* **2021**, *10*, 100071.

(15) Cai, J.; Xu, D.; Dong, Z.; Yu, X.; Yang, Y.; Banks, S. W.; Bridgwater, A. V. Processing thermogravimetric analysis data for isoconversional kinetic analysis of lignocellulosic biomass pyrolysis: Case study of corn stalk. *J. Renew. Sustain. Energy Review.* **2018**, *82*, 2705−2715.

(16) Dejong, W.; Dinola, G.; Venneker, B.; Spliethoff, H.; Wojtowicz, M. TG-FTIR pyrolysis of coal and secondary biomass fuels: determination of pyrolysis kinetic parameters for main species and NO_x precursors. *J. Fuel* **2007**, *86*, 2367−2376.

(17) Liu, J.; Ma, J.; Luo, L.; Zhang, H.; Jiang, X. Pyrolysis of superfine pulverized coal. part 5. thermogravimetric analysis. *J. Energy Convers. Manag.* **2017**, *154*, 491−502.

(18) Geng, C.; Li, S. Y.; Yue, C. T.; Ma, Y. Pyrolysis characteristics of bituminous coal. *J. Energy Convers. Manag.* **2016**, *89*, 725.

(19) Du, R.; Wu, K.; Zhang, L.; She, Y.; Xu, D.; Chao, C.; Qin, X.; Zhang, B. Thermal behavior and kinetic study on the pyrolysis of Shenfu coal by sectioning method. *J. Therm. Anal. Calorim.* **2016**, *125*, 959−966.

(20) Wu, F.; Wang, M. H. Research on the pyrolysis characteristic and kinetics of Xinjiang bituminous coals. *J. China Coal* **2019**, *45*, 84−90.

(21) Ma, Y.-y.; Wang, H.-h.; Mo, W.-l.; Zhang, X.-y.; Fan, X.; Ma, J.; Ma, F.-y.; Wei, X.-y. Effect of swelling by organic solvent on structure, pyrolysis and methanol extraction performance of Hefeng bituminous Coal. *J. ACS Omega* **2021**, *6*, 14765−14773.

(22) Liang, S.; Hou, Y.; Wu, W.; Li, L.; Ren, S. New Insights into the primary reaction products of Naomaohu coal via breaking weak bonds with supercritical ethanolysis. *J. Energy Fuel.* **2019**, *33*, 6294−6301.

(23) Liu, W. Y.; Du, M. H.; Qu, S. J.; Shi, S. D. Study on pyrolysis kinetics of Shenhua coal direct liquefaction residue. *J. Coal Sci.* **2006**, *2*, 215−218.

(24) Liu, Q.; Wu, K.; Du, R.; She, Y.; Liu, X. Kinetic analysis of tar's separation from lump Coal. *ISIJ Int.* **2015**, *55*, 947−951.

(25) Wang, T.; Li, C.; Zhou, B.; Zhang, Y.; Zhang, M.; Yang, H.; Wang, Z. Experimental investigation of thermal effect in coal pyrolysis process. *ISIJ Int.* **2020**, *200*, 106269.

(26) Wang, Y.; Zhang, Y.; Zhou, Q.; Zhang, Y.; Sun, J. Thermal kinetics analysis of coal-gangue selected from Inner Mongolia in China. *J. Therm. Anal. Calorim.* **2018**, *131*, 1835−1843.

(27) Lv, S.; Lv, G. J.; Jiang, X. G.; Cui, C.; Yan, J. H.; Cen, K. F.; Yu, X. H.; Liao, H. Y.; Zhao, H. Pyrolysis/combustion characteristics and kinetic analysis of Indonesia lignite sludge. *J. China Coal Soc.* **2014**, *39*, 554−561.

(28) Jain, A. A.; MehraRanade, A. V. V. Processing of TGA data: analysis of isoconversional and model fitting methods. *J. Fuel* **2016**, *165*, 490−498.

(29) Ma, Y. Y.; Ma, F. Y.; He, F.; Sun, Z. Q.; Mo, W. L.; Zhang, X. J. Influence of microwave swelling with cavitated creosote oil on the direct liquefaction performance of Xigou coal from Xinjiang and its dynamics analysis. *J. China Coal Soc.* **2017**, *42*, 2733−2741.

(30) Czajka, K.; Kisiela, A.; Moroń, W.; Ferens, W.; Rybak, W. Pyrolysis of solid fuels: thermochemical behaviour, kinetics and compensation effect. *ISIJ Int.* **2016**, *142*, 42−53.

(31) Skodras, G.; Nenes, G.; Zafeiriou, N. Low rank coal-CO_2 gasification: experimental study, analysis of the kinetic parameters by Weibull distribution and compensation effect. *J. Appl. Therm. Eng.* **2015**, *74*, 111−118.

(32) Marbán, G.; Laura, R. Tentative explanation for the kinetic compensation effect in doped catalysts. *J. Kinet. Catal.* **2013**, *54*, 487−492.

(33) Meng, D.; Wang, T.; Xu, J.; Chen, X. Diffusion effect and evolution of kinetic parameters during coal char-CO_2 gasification. *J. Fuel* **2019**, *255*, 115819.

(34) Rasam, S.; Moshfegh Haghighi, A.; Azizi, K.; Soria-Verdugo, A.; Keshavarz Moraveji, M. Thermal behavior, thermodynamics and kinetics of co-pyrolysis of binary and ternary mixtures of biomass through thermogravimetric analysis. *J. Fuel* **2020**, *280*, 118665.

(35) Ma, Y.-y.; Ma, F.-y.; Mo, W.-l.; Wang, Q. Five-stage sequential extraction of Hefeng coal and direct liquefaction performance of the extraction residue. *J. Fuel* **2020**, *266*, 117039−117048.

(36) Wang, Y.; Ma, Y. Y.; Mo, W. L.; Gong, W. T.; Ma, F. Y.; Fan, X.; Wei, X. Y.; Zhang, S. P. Functional groups of sequential extracts

https://doi.org/10.1021/acsomega.2c00307
ACS Omega 2022, 7, 21397−21406

and corresponding residues from Hefeng sub-bituminous coal based on FT-IR analysis. *J. Fuel Chem. Technol.* **2021**, *49*, 890.
(37) Sarwar, A.; Nasiruddin Khan, M.; Azhar, K. F. Kinetic studies of pyrolysis and combustion of Thar coal by thermogravimetry and chemometric data analysis. *J. Therm. Anal. Calorim.* **2012**, *109*, 97−103.

https://doi.org/10.1021/acsomega.2c00307
ACS Omega 2022, 7, 21397−21406